Filled skutterudite $CeFe_4As_{12}$: Disclosure of a semiconducting state

R. Wawryk, Z. Henkie, A. Pietraszko, T. Cichorek, and L. Kępiński
Institute of Low Temperature and Structure Research, Polish Academy of Sciences, PL-50-950 Wrocław, Poland

A. Jezierski and J. Kaczkowski
Institute of Molecular Physics, Polish Academy of Sciences, PL-60-179 Poznań, Poland

R. E. Baumbach and M. B. Maple
Department of Physics, University of California San Diego, La Jolla, California 93740, USA
(Received 20 May 2011; revised manuscript received 16 August 2011; published 10 October 2011)

Crystals of the filled skutterudite compound $CeFe_4As_{12}$ with three different types of morphology and charge carrier concentration were grown by a molten Cd:As flux method. X-ray diffraction, magnetization, specific heat, electrical resistivity, Hall coefficient, and thermoelectric power measurements on these materials, as well as band structure calculations, are presented that reveal phenomena that are associated with *f*-electron-conduction electron hybridization and heavily doped semiconductors. Valence fluctuations or Kondo behavior dominate the physics above $T \sim 280$ K. The correlated electron behavior is manifested at low temperatures as a hybridization-gap insulating state. The small activation energy $\Delta_3/k_B \sim 165$ K, taken from fits to electrical resistivity data, correlates with the evolution of a weakly magnetic or nonmagnetic ground state, which is evident in the magnetization data below a coherence temperature $T_{coh} \sim 90$ K. Additionally, the low-temperature electronic specific heat coefficient is small, $\gamma \sim 3.3$ mJ/mole K^2. A prediction of an *f*-electron-character free wide parabolic-like top of the valence band is consistent with heavily doped semiconductor features of electron transport properties.

DOI: 10.1103/PhysRevB.84.165109 PACS number(s): 75.30.Mb, 71.30.+h, 71.20.−b, 71.55.Ak

I. INTRODUCTION

The ternary transition metal pnictides with the chemical formula MT_4X_{12} ($M =$ alkali metal, alkaline earth, lanthanide, actinide; $T =$ Fe, Ru, Os; $X =$ P, As, Sb), which crystallize in the filled skutterudite structure (space group *Im3*), exhibit a wide variety of strongly correlated electron phenomena.[1–4] Many of these phenomena depend on hybridization between the rare-earth or actinide *f*-electron states and the conduction electron states which, in some filled skutterudite systems, leads to the emergence of semiconducting behavior. This trend is evident in the cerium-transition metal phosphide and antimonide systems, most of which are semiconductors, where the gap size is correlated with the lattice constant.[5–7] Although many of these systems have been studied in detail, the arsenide members have received little attention, probably because of difficulties associated with their synthesis. Our recent interest has focussed on the effect of hybridization in CeT_4As_{12} skutterudites.

For the family of CeT_4As_{12} compounds, the clearest picture emerges for $CeOs_4As_{12}$. Here, a hybridization gap insulating state is observed, as evinced by an increase in the electrical resistivity $\rho(T)$ by over two orders[8] of magnitude and a decrease in the carrier concentration by over three orders[9] of magnitude, upon cooling below 0.1 K. A small energy gap $\Delta/k_B \sim 73$ K, taken from fits to $\rho(T)$, characterizes the strength of the hybridization and correlates with the evolution of a weakly magnetic or nonmagnetic ground state. For $CeRu_4As_{12}$, a hybridization gap insulating state ($\Delta/k_B \sim$ 50 K[10]) was reported for polycrystalline specimens, while single crystals (grown from Cd:As flux) reveal non-Fermi-liquid behavior associated with a nonmagnetic ground state.[11] Finally, semimetallic[12] and semiconducting ($\Delta/k_B \sim 116$ K)[13] behaviors have been reported for polycrystalline samples of $CeFe_4As_{12}$, while band structure calculations[14] predict a forbidden gap of 2760 K. Our recent work showed that both semimetallic and semiconducting single crystals can be grown via the Cd:As flux growth method.[15] In this article, we report further results for $CeFe_4As_{12}$ single crystals that were synthesized using the Cd:As flux growth method. These specimens show three distinct morphologies with differing types of behavior. Measurements of the electrical resistivity ρ, longitudinal magnetoresistivity ($\Delta\rho/\rho$), magnetization M, specific heat C, Hall coefficient R_H, thermoelectric power S, and band structure calculations show that $CeFe_4As_{12}$ has a nonmagnetic or weakly magnetic semiconducting ground state with semimetallic properties, when unintentionally (but heavily) doped.

II. EXPERIMENTAL DETAILS

Single crystals of $CeFe_4As_{12}$ were grown from elements with purities >99.9%, by mineralization in a molten Cd:As flux at high temperatures and pressures, as described previously.[16] Two different crystal-growth experiments were performed where the Ce content was varied; i.e., the elemental components were combined in the atomic ratio Ce:Fe:Cd:As = 0.85:4:12:48 ($Ce_{0.85}Fe_4As_{12}$ + 12 $CdAs_3$) for the first experiment (A), and Ce:Fe:Cd:As = 1.15:4:12:48 ($Ce_{1.15}Fe_4As_{12}$ + 12 $CdAs_3$) for the second experiment (B). The subsequent growth procedures were the same for both experiments. The starting materials were sealed in pyrolized quartz ampoules, heated to 820 °C at a rate of 20 °C/hr and repeatedly heated/cooled between 820 and 780 °C for six weeks at a rate of 3 °C/hr. Finally, the ampoules were cooled to room temperature at a rate of 20 °C/h. The heating was done in a homebuilt high-pressure cell filled with 19 atm

 ©2011 American Physical Society

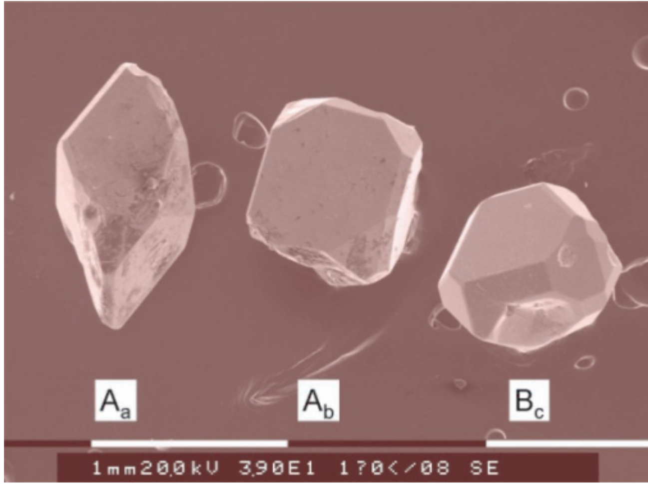

FIG. 1. (Color online) Three types of characteristic forms of $CeFe_4As_{12}$ crystals: A_a with elongated diamond-shaped faces; A_b with rectangular shape of the largest faces; B_c with isometric forms with many faces.

of Ar pressure, which is approximately equal to the estimated vapor pressure of the $CdAs_3$ flux in the ampoule at 820 °C. The main purpose of the Ar is to balance the pressures inside and outside the inner ampoule and thereby avoid an explosion. The solidified flux was removed from the $CeFe_4As_{12}$ crystals by means of sublimation in high vacuum at 600 °C.

The $CeFe_4As_{12}$ crystals obtained had different forms and dimensions (Fig. 1). Those with sizes of approximately 1 mm were cleaned in acid to remove a possible cerium arsenide impurity phase from the surface of the crystals.

Two different types of $CeFe_4As_{12}$ crystals (labeled A_a and A_b) were found for batch A. The majority of these specimens (A_a) has an elongated form with well-developed diamond-shaped faces. The minority phase (A_b) consists of crystals with roughly rectangular shapes. Crystals of an isometric form, with many faces, were only found for batch B (labeled B_c). Representative specimens for each type of morphology were examined using an electron microscope with EDS analysis. X-ray diffraction (XRD) data were taken with a four-circle x-ray diffractometer, where the measurement was made using a two-dimensional CCD detector. All morphologies were examined at room temperature. Additionally, specimens with the A_a and A_b morphologies were examined at 12 K by XRD. Their structures were resolved by means of the full-matrix-least-squares method using the SHELX-97 program.[17,18] X-ray powder diffraction measurements were performed using an X'Pert PRO PANAlytical machine on a powder that was prepared by grinding single crystals. The dc magnetization (M) was measured for collections of randomly oriented single-crystals with the total mass of 0.4 g using a SQUID magnetometer (Quantum Design, Inc.). The electrical resistivity (ρ), longitudinal magnetoresistivity ($\Delta\rho/\rho$), and Hall resistivity (R_H) were measured in a standard four-wire configuration in the range 0.3 K < T < 300 K for single crystalline specimens in a ^{3}He cryostat, using an ac resistance bridge. Measurements of the thermoelectric power (S) for 0.5 K < T < 350 K were performed on single crystals with lengths ~1 mm using a method described in Ref. 19. Specific heat measurements (C)(were performed for collections of crystals with total masses between 14 and 20 mg.

III. RESULTS

The XRD analysis shows that all of the $CeFe_4As_{12}$ crystals, regardless of their morphology and physical properties, have the same cubic $LaFe_4P_{12}$-type (*Im3* space group) structure at room temperature. Moreover, no change in structure is observed for the A_a and A_b specimens down to 12 K. For A_a crystals, only an inspection of the x-ray powder diffraction background reveals several weak peaks, indicative of less than 1% of an unidentified impurity phase. A summary of the crystal structure data and some basic physical parameters are given in Tables I and II, respectively.

The following quantities are listed in the table: a (Å) is the unit cell parameter, the atomic coordinates x, y are given for As atoms (x, y, and z are equal to 0 for Ce and 0.25 for Fe, while $z = 0$ for As); O are the occupancy factors for the Fe, As, and Ce atoms; $l_{Ce,Fe:As}$ (Å) are the chemical bond lengths Ce-As and Fe- As, D (Å^2 × 10^3) are the displacement parameters for atoms Fe, As, Ce, df denotes $R1/wR2$—the final discrepancy factors in %, and CeL, (Fe/Os)K, and AsK denote contents of Ce, Fe or Os, and As in atomic percent units, determined on the basis of L or K lines, respectively.

The XRD data shown in Table I were taken (on the same diffractometer) for representative specimens of each type of crystal morphology. These results show that the lattice constant a is the same for all types of crystals with an average value of $a \sim 8.301(2)$ Å. This value can be compared to $a = 8.2959$ Å (see Ref. 13) and 8.296 Å,[12] as reported previously for various polycrystalline specimens. The displacement parameter D represents the average displacement of an atom vibrating around its lattice position and is equal to the mean-square displacement along the Cartesian axes. The displacement parameters of the Ce atoms are more than twice that of the other atoms in the lattice. By considering sums of the occupation factors O, it appears that the vacancies per formula unit are 0.22, 0.47, and 0.16 for crystals 2, 5, and 9, respectively. These values greatly exceed the residual carrier densities (Table II) and do not scale with them.

TABLE I. Crystal structure data of the $CeFe_4As_{12}$ specimens with three types of morphology.

$CeFe_4As_{12}$	No. 2 - B_c	No. 5 - A_a	No. 9 - A_b	$CeOs_4As_{12}$
a	8.303(2)	8.302(2)	8.299(2)	8.519(2)
x	0.1543(2)	0.1549	0.1543	0.1485
y	0.3445(2)	0.3439	0.3445	0.3485
O_{Fe}	1.000(20)	0.967(20)	1.000(20)	1.00
O_{As}	0.983(20)	0.972(20)	0.988(20)	1.00
O_{Ce}	0.985(20)	1.000(20)	0.983(20)	0.99
$l_{Ce,As}$	3.1342	3.1311	3.1326	3.2273
$l_{Fe,As}$	2.3572	2.3533	2.3559	2.4470
D	1; 2; 7	0; 1; 6	2; 3; 8	3; 4; 12
df	6.55/12.8	11.7/25.6	4.47/8.35	4.02/11.0
CeL	6.27(10)	6.29(17)	6.30(12)	6.42(11)
(Fe/Os)K	24.71(19)	24.33(42)	24.48(27)	26.60(25)
AsK	69.02(26)	69.38(51)	69.22(33)	66.97(25)

TABLE II. Crystals of $CeFe_4As_{12}$ that were examined are identified by the label number (No.), a type of shape shown in Fig. 1, the unit cell parameters *a*, the number of formula units per volume *N*, a residual density of charge carriers (holes) p_H, and a sign of temperature coefficient of resistivity δ below 165 K.

No.	Shape	*a* (294 K) (Å)	*a* (12 K) (Å)	*N* (f.u./cm^3)	p_H (4.2 K) (e$^+$/cm^3)/(e$^+$/f.u.)	δ for T< 165 K
2	B_c	8.303(2)	...	3.5×10^{21}	$1.0\times10^{20}/0.031$	negative
4	A_a	8.302(3)	...	...	...	negative
5	A_a	8.2946(5)	8.2741(8)	...	$1.5\times10^{20}/0.042$	negative
6	A_b	8.289(2)	...	...	...	positive
8	A_b	8.2759(2)	8.2596(12)	3.5×10^{21}	$2.9\times10^{20}/0.094$	positive
9	A_b	8.303(2)	...	...	...	positive

The chemical contents, determined via EDS measurements on polished specimens, and given in Table I were obtained by averaging over 24 points along the surface of each specimen. Here, the uncertainty represents the largest differences between measured content for different points along the surface. The greatest differences in the elemental content of Ce, Fe, and As are equal to 0.5, 1.5, and 0.5%, respectively, and are lower than the differences in the elemental content suggested by the occupation factors. Analysis of various $CeFe_4As_{12}$ crystals showed that, within the experimental error, there is no difference in elemental composition between specimens. However, the measured composition differs from that of the ideal formula (Ce 5.88 at.%, Fe 23.53 at.%, As 70.59 at.%). Similar differences were previously observed for $CeOs_4As_{12}$ specimens (the Ce content was higher than expected), where the increase of the resistivity over two orders[8] of magnitude and the decrease of Hall carrier concentration [from 7×10^{20} to 1.5×10^{17}e$^+$/cm^3 (Ref. 9)] with decreasing temperature suggest a low density of stoichiometric defects. If we assume that the composition of a typical $CeOs_4As_{12}$ sample is fixed, then it seems likely that the EDS analysis gives a systematic error, although differences of the elemental content may still be informative for samples composed of the same elements. The sum of the highest difference of a particular element content, equal to 0.12 atoms/f.u., can be compared to 0.06 e$^+$/f.u., which is the difference between densities of carriers in crystals 9 and 2. These values are reasonably close to each other, if we take into account the possible partial compensation of acceptors (majority) by donors, which might be produced by stoichiometric defects.

The dc magnetic susceptibility data measured at $H = 5$ kOe for $CeFe_4As_{12}$ crystals with the A_a and B_c morphologies are shown in Fig. 2. For comparison, the magnetic susceptibility of $LaFe_4As_{12}$ is displayed in the right inset of Fig. 2 (details are presented in Ref. 20). For $CeFe_4As_{12}$, the $\chi(T)$ data shows a weak and unusual T dependence, i.e., $\chi(T)$ decreases with decreasing temperature, displaying a reduction in slope at about 280 K. Below this temperature and down to around 90 K, the $\chi(T)$ curves continue to decrease with a slightly convex shape. Whereas the T dependence of the magnetic susceptibility suggests a maximum at $T > 400$ K, a sample-dependent upturn was observed below 60 K.

For the A_a crystals, the upturn is arrested by a peak at 2.4 K, with $\chi(2.4\,\mathrm{K}) = 1.42 \times 10^{-3}$ cm^3/mole. For the B_c crystals, the upturn persists to the lowest temperatures measured approaching a value of $\chi(1.7\,\mathrm{K}) = 0.97 \times 10^{-3}$ cm^3/mole. The similarity between the A_a and B_c crystals for $T > 60$ K suggests that the low-T differences are extrinsic in origin; i.e., they are the result of paramagnetic impurities. We also note that $\chi(T)$ for the B_c crystals is lower than that of A_a. Therefore we conclude that the $\chi(T)$ data for B_c crystals is closer to the intrinsic magnetic behavior of $CeFe_4As_{12}$ than those of the A_a crystals.

Various zero-field temperature dependencies of the electrical resistivity $\rho(T)$ for three types of $CeFe_4As_{12}$ single crystals are depicted in Fig. 3. Interestingly, only at lower temperatures, i.e., below $T \approx 225$ K, is the striking sample dependence observed. For $T > 225$ K, the $\rho(T)$ behavior is almost identical for all crystals. Indeed, both the room-temperature value of ρ_0 (320 $\mu\Omega$ cm) and the temperature coefficient of the resistivity $\delta = (1/\rho)(\partial\rho/\partial T)$ are the same.

Upon further cooling, although δ remains positive, $\rho(T)$ differs for each type of crystal; i.e., $\rho(T)$ reaches minimum values of 208 $\mu\Omega$cm at $T_{\min} = 168$ K for B_c-type crystals

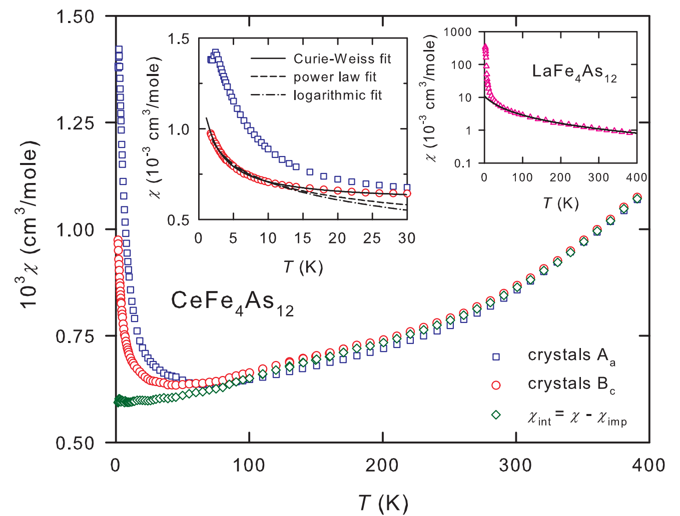

FIG. 2. (Color online) Magnetic susceptibility vs temperature for different collections of $CeFe_4As_{12}$ crystals measured in a field of $H = 5$ kOe. Also shown is the intrinsic magnetic susceptibility $\chi_{int}(T)$ (diamonds) for which a Curie-Weiss (C-W) impurity contribution has been subtracted as defined in the text. *Left inset*: fits to the low-T $\chi(T)$ data described by various equations. *Right inset*: $\chi(T)$ for $LaFe_4As_{12}$ measured in $H = 1$ kOe. The solid line represents a C-W dependence, whose parameters were estimated from the fit to the experimental data above 100 K.

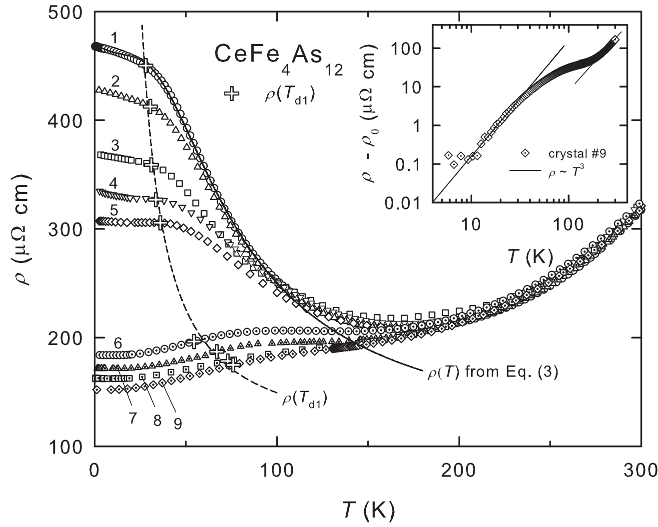

FIG. 3. Electrical resistivity vs temperature for various $CeFe_4As_{12}$ single crystals. The solid line represents a fit of Eq. (3) to the low-T resistivity data for crystal 1. The dashed $\rho(T_{d1})$ line serves as a guide to the eye. *Inset:* A log-log plot of $(\rho - \rho_0)$ vs T for the crystal 9. The solid lines correspond to a $\rho \sim T^3$ dependence.

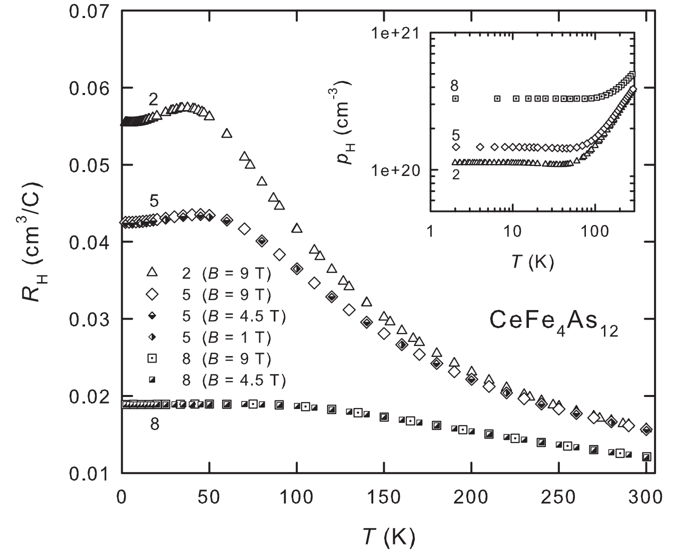

FIG. 4. Hall coefficient vs temperature for three $CeFe_4As_{12}$ single crystals with different sign of δ below 165 K: crystal 8 ($\delta > 0$), and crystals 2 and 5 ($\delta < 0$) measured in fields 1, 4.5, and 9 T. The inset presents the carrier concentrations vs temperature for the above crystals.

(Nos. 1 and 2) and 209–218 $\mu\Omega$cm at $T_{\min} = 165$ K for A_a-type (Nos. 3–5) crystals or a plateau near 206–188 $\mu\Omega$ cm at 120 K for A_b-type (Nos. 6–9) crystals. There is an upturn in $\rho(T)$ for A_a and B_c type crystals below roughly 165 K, with increasing $|\delta|$ and decreasing temperature, until a rapid reduction of $|\delta|$ is seen below a characteristic temperature T_{d1} [defined later: see Sec. IV, Fig. 9(a)], while the resistivity tends to a finite value ρ_0 for $T \to 0$. We emhasize that for the A_b and B_c crystals virtually the same specific-heat data were found (not shown). This holds true for both a value of the Sommerfeld coefficient of the electronic specific heat, $\gamma = 3.3(\pm 0.1)$ mJ/K^{2}mole and the Debye temperature $\Theta_D = 580$ K. It is worth noting that no anomaly in $\rho(T)$ at 2.4 K is observed for A_a type crystals, in contrast to magnetic susceptibility data.

The low-temperature $\rho(T)$ behavior for crystals 1–5 can be described as follows; ρ_0 and $|\delta|$ decrease while T_{d1} increases for increasing crystal number. The low-temperature $\rho(T)$ behavior for A_b-type (Nos. 6–9) crystals can be described in the same way, if we denote by T_{d1} the temperature around which δ rapidly increases when the sample is cooled below the low-temperature side of the plateau in $\rho(T)$. Thus, for increasing sample number, the plateau becomes increasingly less visible, but remains distinct in plots of $\log_{10}(\rho - \rho_0)$ versus $\log_{10}T$, as shown in the inset of Fig. 3. Two ranges of T^3 dependence of resistivity are observed: i.e., below 25 K and above 200 K. These regions are separated by a temperature interval where the electrical resistivity exhibits a weaker T dependence. We also note that the longitudinal magnetoresistivity, $|\Delta\rho/\rho|$ at $T = 2$ K and $B = 9$ T is less than 0.1% for all three types of $CeFe_4As_{12}$ single crystals. This behavior is strikingly different from that one observed for the hybridization-gap semiconductor $CeOs_4As_{12}$ where already $B = 3$ T closes the smallest energy gap, resulting in large variations in the electrical resistivity with magnetic field.[8]

Measurements of the Hall effect were performed for crystals 2, 5, and 8, which represent the three types of morphologies. The Hall coefficients, determined for 2 K $\leqslant T \leqslant$ 300 K in magnetic fields $B = 1$, 4.5, and 9 T are presented in Fig 4. For all types of crystals, the Hall coefficient is positive and independent of magnetic field. R_H increases weakly with decreasing temperature for crystal 8 until saturating near 0.0217 cm^3/C for 2 K $\leqslant T \leqslant$ 90 K. The increase of R_H is stronger for crystals 2 and 5, and reaches a cusp localized near 38 and 45 K, respectively, and subsequently saturates at slightly lower values at lower temperatures. An analysis of dR_H/dT versus $\log_{10}T$ indicates that T_{d1} varies for crystals 2, 5, and 8; $T_{d1} = 30.5$, 36, and 73 K, respectively. In the single-band approximation, $R_H = 1/p_H e$, from which the carrier concentrations at room temperature and low temperature [p_H(300 K):p_H(2 K)] can be estimated. In units of e$^+$/f.u., this formula gives carrier concentrations 0.098:0.028, 0.114:0.042, and 0.128:0.082 for crystals 2, 5, and 8, respectively. Here, the density of an f.u. is 3.5×10^{21} f.u./cm^3. These results indicate that our crystals have semimetallic or degenerate semiconductor ground states.

The thermoelectric power versus temperature data for crystals 1, 5, and 8, representing the three types of $CeFe_4As_{12}$ crystals, [B_c; No. 1 ($\delta < 0$), A_a; No. 5 ($\delta < 0$), and A_b; No. 8 ($\delta > 0$)], is shown in Fig. 5. A large hump is observed in $S(T)$, with $S_{\max} \sim 86$, 75, and 57 μV/K at $T_{\max}$ of 120, 130, and 155 K for crystals 1, 5, and 8, respectively. Another feature that is common to all of the curves is a shallow valley where $S_{\min} = 46$, 51, and 47 μV/K centered at $T_{\min} \approx 340$, 330, and 305 K for crystals 1, 5, and 8, respectively.

Below $T_{\max}$, $S(T)$ decreases with decreasing temperature to a characteristic temperature $T^* \approx 68$ K, below which $S(T)$ tends strongly toward zero with decreasing T for crystals 1 and 5 ($\delta < 0$ are solid and dashed lines in Fig. 5). In contrast, crystal 8 exhibits a sign change near 4 K and a subsequent weak valley ($\delta > 0$ is dashed-dotted line in Fig. 5). It is expected that

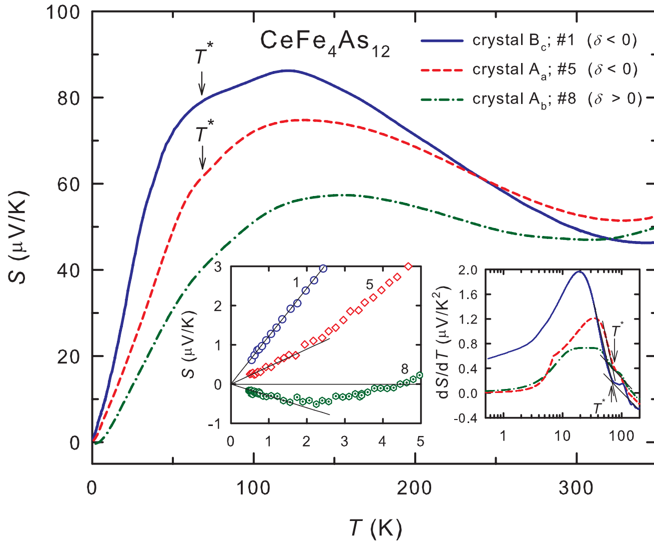

FIG. 5. (Color online) Thermoelectric power vs temperature for $CeFe_4As_{12}$ crystals: No. 1 ($\delta < 0$ is a solid line), No. 5 ($\delta < 0$ is a dashed line), and No. 8 ($\delta > 0$ is a dashed-dotted line). The left inset displays low-T $S(T)$ data for the above crystals. The right inset shows the derivative $\mathrm{d}S/\mathrm{d}T$ vs $\log_{10}T$.

S and R_H should yield the sign of charge carriers, based on Eq. (8). Our results for S and R_H imply that the sign of charge carriers is positive, except for sample 8 for $T < 4$ K where the sign of charge carriers is ambiguous (S and R_H have opposite signs).

Calculation of the electronic band structure of $CeFe_4As_{12}$ was carried out by means of the full-relativistic local-orbital (FPLO-9) method within the local density approximation.[21,22] The exchange correlation potential was used in the form of Perdew and Wang.[23] We have performed the calculations with (full relativistic) and without (scalar-relativistic) spin-orbit interaction. In this work, we present the results for the full-relativistic case. The self- consistent band calculations were carried out on a k mesh of 833 and 1256 k points in the irreducible Brillouin zone (IBZ). The number of k points influences the value of the density of states at the Fermi level. Shown in Fig. 6 is the calculated band structure near the Fermi level for $CeFe_4As_{12}$ with an experimental value of $a = 8.289$ Å. Whereas our results are consistent

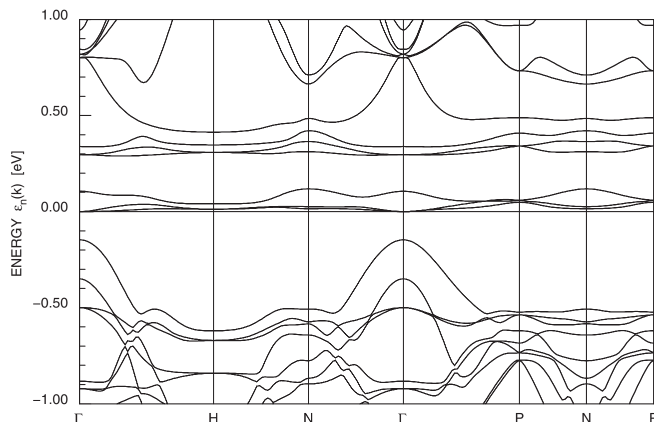

FIG. 6. Calculated band structure for $CeFe_4As_{12}$ with $a = 8.289$ Å.

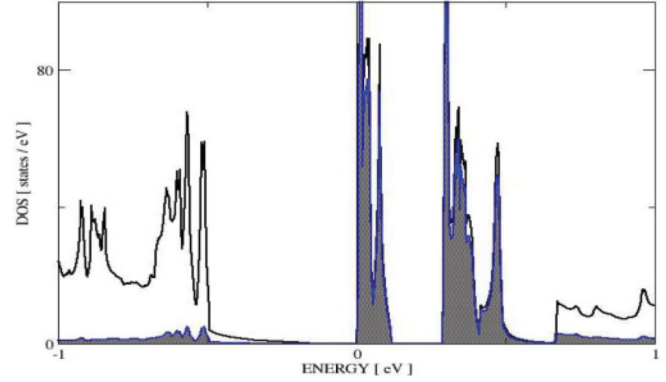

FIG. 7. (Color online) Total density of states for $CeFe_4As_{12}$ in the vicinity of the Fermi level E_F. The shaded part of the DOS shows the $4f$ component from Ce.

with previous WIEN2k calculations for $CeFe_4As_{12}$,[14] some additional information has been obtained by these calculations; a direct energy gap E_g of about 0.147 eV is formed at the Γ point, where maxima of two valence bands with parabolic-like structures are found. The top of the lower valence band is located about 0.4 eV below the lowest conduction band. While the Ce-$4f$ character dominates the lower valence-band structure at Γ, there is mainly Fe-$3d$ character when going toward the zone boundary. Most importantly, near the Fermi level we observe strong hybridization between Ce-$4f$, Fe-$3d$, and As-$4p$ states that form conduction bands. The lowest lying conduction bands are dominated by the narrow spin-orbit split band, which is mainly formed by the $4f$ electron state of Ce. These two flat bands are separated by an indirect band gap of about 0.5 eV, with the top of the lower band at the N point.

In Fig. 7, we show the full relativistic densities of states DOS for $CeFe_4As_{12}$. The shaded area indicates the contribution of $4f$ electron states from the Ce atoms. The energy gap below the Fermi level is clearly determined by the direct gap mentioned above. Since the Fermi level is located on the left side of Ce-$4f$ peak, even a very small shift of its position may lead to significant variation of physical properties. Our self-consistent calculations have shown that cerium has 1.06 electrons of the $4f$ type as well as calculations performed for 833 k-points in the IBZ give the density of states at the Fermi level $N(E_F) = 0.605$ (states/eV f.u) ($\gamma = 1.42$ mJ/K^2 mole) and for 1256 k points in the IBZ give $N(E_F) = 4.674$ (states/eV f.u) ($\gamma = 10.99$ mJ/K^2 mole). The reason of such a change is due to the location of the Fermi level on the left side of sharp peak associated with the $4f$ electrons.

Finally, we have also studied the influence of the lattice parameter on the value of the direct energy gap E_g at the Γ point for $CeFe_4As_{12}$. The results are presented in Fig. 8, where the lattice parameter a varies from 8.050 to 8.45 Å. From the calculations performed for scalar relativistic and full-relativistic cases, we conclude that a significant decrease of the energy gap is expected with increasing a. These results are in qualitative agreement with the general relationship between the energy gap and lattice parameter of the Ce-based skutterudite compounds.[24]

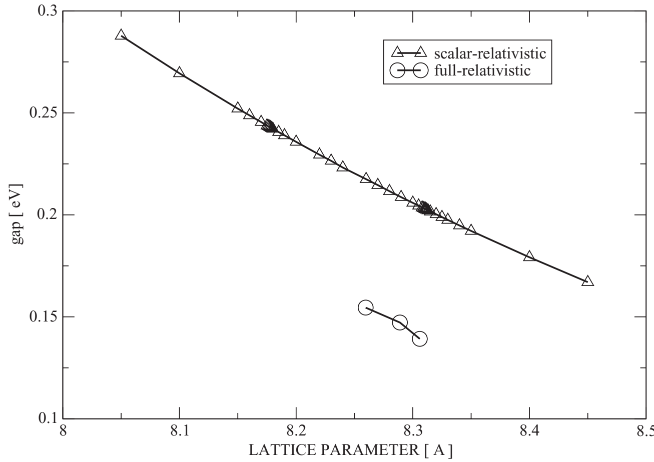

FIG. 8. Variation of the main energy gap E_g at the Γ point as a function of lattice parameter a for $CeFe_4As_{12}$ determined for the scalar-relativistic (triangles) and full-relativistic cases.

IV. DISCUSSION

Taken together, the x-ray diffraction, $M(H,T)$, $C(T)/T$, $\rho(T)$, $R_H(T)$, $S(T)$, and band structure calculations indicate that hybridization between the Ce *f*-electron states and the conduction electron states dominates the physics of $CeFe_4As_{12}$, yielding a variety of types of behavior that are roughly divided into several temperature regions.

For $T > 100$ K, the unusual behavior is most pronounced in the $\chi(T)$ data, which deviate from the typical Curie-Weiss dependence expected for Ce^{3+} ions: i.e., $\chi(T)$ decreases with decreasing T for $T > 100$ K, below which a sample-dependent upturn is observed that may originate from paramagnetic impurity ions. We attempted to quantify the putative impurity contribution for the B_c crystals by considering a modified Curie-Weiss (C-W) expression:

$$\chi(T) = \chi_0 + C_{imp}/(T - \Theta_D), \tag{1}$$

where $\chi_0 = 0.597 \times 10^{-3}$ cm^3/mole, $C_{imp} = 1.308 \times 10^{-3}$ cm^{3}K/mole, and $\Theta_p = -1.7$ K. We then estimated the intrinsic magnetic susceptibility χ_{int} by considering the expression $\chi_{int}(T) = \chi(T) - \chi_{imp}(T)$ (diamonds in Fig. 2). From this treatment, we suggest that $\chi_{int}(T)$ has a small value at low T [$\chi_{int}(0) = 0.60$ cm^3/mole], which remains nearly T independent for $T < 50$ K, increases gradually in the range 50 K $< T <$ 280 K (with a small inflection point near 90 K), and finally increases more rapidly above 280 K. We note that this behavior is similar to what is observed for $CeOs_4As_{12}$ and $CeRu_4As_{12}$, where the high-T increases in rate are observed above 135 [8] and 90 K, respectively.[11]

There are two models that describe such an evolution in $\chi(T)$. The first is the intermediate valence picture, where the Ce ions have dynamic temporally fluctuating valences, in this case between 3+ (magnetic) and 4+ (nonmagnetic), which evolve into a nonmagnetic ground state with an enhanced Pauli-like magnetic susceptibility below the valence fluctuation temperature T_{vf}. The second scenario is the Kondo lattice picture, where the magnetic moments of the Ce^{3+} ions are screened by the conduction electrons through a negative exchange interaction, resulting in a nonmagnetic ground state below the Kondo temperature T_K.

In the intermediate valence picture, the ratios $n^{3+}(T)$ and $n^{4+}(T) = 1 - n^{3+}(T)$ describe the fraction of Ce ions in each valence state. The 4*f*-electron shell of each Ce ion temporally fluctuates between the configurations $4f^1$ (Ce^{3+}) and $4f^0$ (Ce^{4+}) at a frequency $\omega \approx k_B T_{vf}/\hbar$, where T_{vf} separates magnetic behavior at high temperatures $T \gg T_{vf}$ and nonmagnetic behavior at low temperatures $T \ll T_{vf}$.[25,26] For Ce^{3+} (one localized 4*f* electron), $\chi(T)$ should behave as a Curie-Weiss law modified by crystalline electric-field splitting, while for Ce^{4+} (no localized *f* electron), $\chi(T)$ should be temperature independent (Pauli susceptibility). In the case of $CeFe_4As_{12}$, $\chi_{int}(T)$ is consistent with an intermediate valence scenario in which T_{vf} is somewhere above room temperature.

On the other hand, it is possible that the Ce ions remain in the 3+ state at all T and the Ce^{3+} magnetic moments are screened via the Kondo interaction below a characteristic temperature T_K. This scenario is commonly called the Kondo picture,[27] and may be appropriate for $CeFe_4As_{12}$ if $T_K >$ 400 K, leading to Curie-Weiss behavior for $T > T_K$ and the observed $\chi(T)$ behavior for 90 K $< T < T_K$. A rough estimate of T_K can be made by using the expression:

$$T_K = N_A \mu_{eff}^2 / 3\chi_0 k_B, \tag{2}$$

where $\mu_{eff} = 2.54\ \mu_B$ is the Hund's rule value for free Ce^{3+} ions and $\chi_0(T = 90\text{ K}) \approx 0.64 \times 10^{-3}$ cm^3/mole or $\chi_0(T = 250\text{ K}) \approx 0.80 \times 10^{-3}$ cm^3/mole is the χ representing the magnetic susceptibility of a screened Kondo ion singlet.[28] The temperature 250 K is just below the high-temperature $\chi(T)$ slope change that corresponds to the saturation value of the susceptibility χ_0 at 135 K for $CeOs_4As_{12}$. By using this rough expression, T_K is found to be near 1000–1260 K, supporting the notion of a high Kondo temperature. For Ce-based Kondo semiconductors, a direct relation between the charge gaps (Δ_C) and T_K is expected, given by $\Delta_C \sim 2k_B T_K$, as proposed in Ref. 29. Thus the expected Δ_C for $CeFe_4As_{12}$ is near 0.170–0.220 eV. This value is consistent with our result from band structure calculations.

The electrical resistivity data also reveal several different regions that approximately mirror the changes in $\chi(T)$. For $T > 150$ K, $\rho(T)$ is nearly identical for all samples and decreases with decreasing T. If we assume that the high T_K scenario is the appropriate description for this system, then the decrease of $\rho(T)$ with decreasing T for 150 K < T < 300 K may reflect the onset of Kondo coherence at $T > 300$ K, in addition to the freezing out of phonons.

For $T < 150$ K, $\rho(T)$ is quite varied, revealing that the low-T electrical transport behavior is sensitive to small perturbations, as seen for $\chi(T)$. Over this T range, $\rho(T)$ for crystals 1–5 increases with decreasing T, but does not follow an Arrhenius equation, which would be appropriate for a simple single-gap semiconductor. Instead, the data are described by a phenomenological three-gap expression,[8,30,31]

$$1/\rho = \sum_i A_i \exp(-\Delta_i / k_B T), \tag{3}$$

where A_3, A_2, and A_1 are equal to 9.11×10^{-3}, 6.08×10^{-5}, and 2.14×10^{-3} ($\mu\ \Omega$ cm)$^{-1}$ and the activation energies

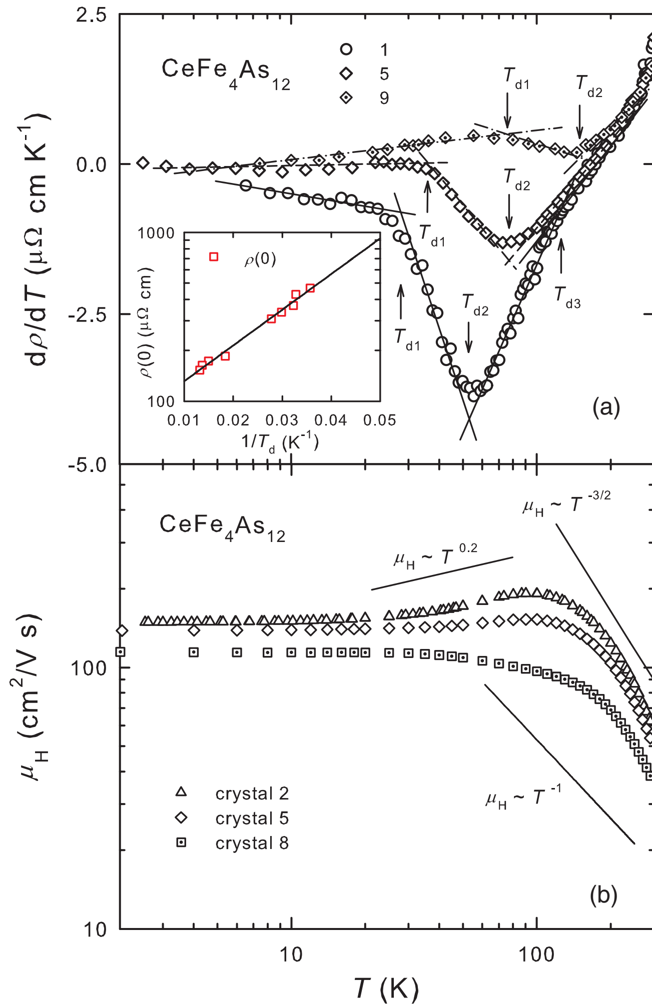

FIG. 9. (Color online) (a) The derivatives $d\rho/dT$ vs T (log scale) for crystals Nos. 1, 5, and 9 of $CeFe_4As_{12}$. T_{d1}, T_{d2}, and T_{d3} denote the characteristic temperatures defined in the text. Displayed in the inset is a plot of $\rho(0)$ vs $1/T_{d1}$. (b) The Hall mobility μ_H plotted as a function of T (on a log-log scale) for $CeFe_4As_{12}$ single crystals marked as Nos. 2, 5, and 8. The straight lines represent the temperature dependencies of the Hall mobility.

Δ_3/k_B, Δ_2/k_B, and Δ_1/k_B are equal to 165, 10.4, and 8×10^{-4} K, respectively. An example of such a fit of Eq. (3) to the $\rho(T)$ data is shown in Fig. 3 for sample No. 1. In contrast, samples Nos. 6–9 do not exhibit increasing $\rho(T)$ with decreasing T. However, as shown in Fig. 9, all samples exhibit three characteristic temperature scales. Here, we consider $d\rho/dT$ versus $\log_{10}T$, as motivated by an earlier example where dS/dT versus $\log_{10}T$ was used to detect temperature ranges with differing conductivity mechanisms. [32,33] We have considered samples Nos. 1, 5, and 9, which represent all three morphologies discussed above. The data trace several roughly linear sections that can be approximated with straight lines. The crossing of the straight lines identify temperatures T_{d1}, T_{d2}, and T_{d3}, which separate the $\rho(T)$ curves into segments in which there are different mechanism of conductivity that are described with different activation energies.

Therefore we infer the following physical meaning for the components of Eq. (3). High doping and very low Δ_1/k_B suggest that the first term is due to hopping of charge carriers between stoichiometric defect states in the gap. Here, the expression $A_1\exp(-D/T^{1/4})$ might be more appropriate if the variable range hopping mechanism dominates conduction for the $0 < T \leqslant T_{d1}$ range.[34,35] The $i = 2$ term describes a contribution to the conductivity due to activation of electrons from the valence band to the acceptor states in the gap. This mechanism dominates within the range $T_{d1} < T \leqslant T_{d2}$.

Finally, there is an activation of electrons from the valence to the conduction band. In the case of activation from the top of a parabolic valence band to the bottom of a parabolic conduction band, the activation energy should be replaced with an energy gap, $\Delta_3/k_B \rightarrow E_g/2k_B$. Therefore

$$1/\rho = A_1 \exp(-D/T^{1/4}) + A_2 \exp(-\Delta_2/k_B T) + A_2 \exp(-E_q/2k_B T). \quad (3a)$$

Best fits of the modified Eq. (3a) were made to $\rho(T)$ data for crystals 1–5 for $0.3 < T < 130$ K ($\approx T_{d3}$). Thus the fitting parameter, E_g, that represents the intrinsic behavior of $CeFe_4As_{12}$ equals 330 K for crystals 1–3 and 440 for crystals 4 and 5. For the two latter crystals, the temperature range of the third contribution to $\rho(T)$ is the most reduced on the low temperature side and the anomaly that defines T_{d3} is substantially reduced. Therefore the value determined for E_g is, most likely, unreliable. The complete form of Eq. (3a) fitted to $\rho(T)$ for crystal No. 1 (solid line) as well as $\rho(T)$ data for all of the crystals examined are presented as $\log_{10}(1/\rho)$ versus $1/T$ plots in Fig. 10 in the range $25 < T \leqslant 300$ K.

The dotted lines represent the sum of the two first contributions in Eq. (3a) and the dash-dotted line represents the third term. The third contribution is the same for crystals 1, 2, and 3, yielding $E_g = 330$ K. The sum of the first two contributions, increasing with increasing crystal number, is presumably responsible for the decreasing slope of the $\log_{10}(1/\rho)$versus $1/T$ dependence of the data. The slope determines an "effective" activation energy: $E^f = 10.4$, 10.0, and 7.7 meV, respectively. Such behavior was previously observed for the conventional semiconductor Th_3As_4.[36] Seven different samples of this semiconductor showed formal energy gaps $E_g{}^f$ ranging from 0.21 to 0.37 eV for conductivity within an exhaustive range increasing from 50 to 290 $(\Omega\ \mathrm{cm})^{-1}$. Optical spectroscopy examination for these samples showed a roughly sample independent indirect gap of $E_g = 0.39$ eV.[37,38]

We now consider the electrical resistivity of the A_b-type crystals (curves 6–9) in more detail. Despite their positive δ over the entire temperature range, they do not show a Bloch-Grüneissen-like temperature dependence. Similar behavior was observed for $CeFe_4Sb_{12}$,[28,39,40] which shows a steplike ρ versus T dependence, which is also sample dependent below 225 K. In our study, the electrical resistivity for crystal 6 reaches the nearly temperature independent value $\sim$206 $\mu\Omega$ cm in the temperature range 160–80 K and then continues to decrease and finally saturates at a residual resistivity $\rho_0 = 185$ $\mu\Omega$ cm below about 30 K. A gradual decrease of the residual resistivity is observed for crystals 7, 8, and 9 and is accompanied by a gradual weakening of the higher temperature step. The step is still clearly seen for crystal 9, which shows the lowest $\rho_0 = 152$ $\mu\Omega$cm, if its $\rho(T)-\rho_0$ versus T data are presented on the log-log plot as shown in

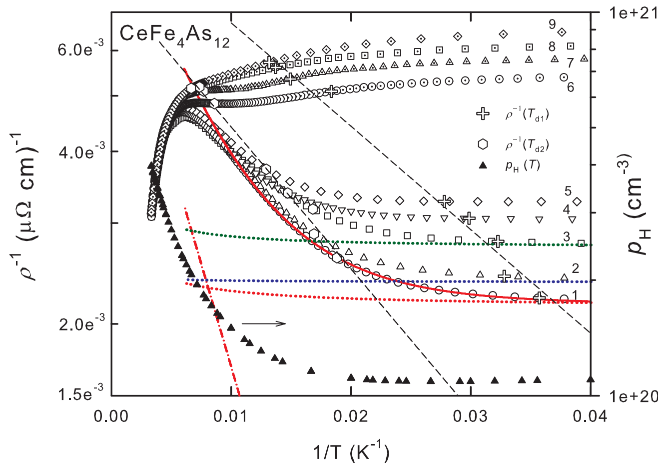

FIG. 10. (Color online) Resistivity data for $CeFe_4As_{12}$ crystals Nos. 1–9 (numbers by curves) for $25 \leqslant T \leqslant 300$ K plotted as $1/\rho$ vs $1/T$ on a log scale. The solid curve that passes through the low temperature data for crystal 1 illustrates the good fit of Eq. (3a) to the total conductivity $(1/\rho)$ of crystal 1. The lowest dotted curve shows the sum of the first two terms of the fit of Eq. (3a) to the $\rho(T)$ data. The two upper dotted curves give the same information for crystals 2 and 3, respectively. The dashed-dotted curve shows term 3 of Eq. (3a) and is the same for crystals 1, 2, and 3 corresponding to E_g = 330 K. The large crosses give conductivities of a particular crystal at the characteristic temperature T_{d1} approximated by the broken straight line representing the fitted Arrhenius equation. The same information is represented by hexagons for characteristic temperature T_{d2}. The filled triangles represent the p_H vs $1/T$ plot on a log scale for crystal 2. The tangent at 300 K corresponds to $E_g = 530$ K [assuming $p_H \sim \exp(-E_g/2k_BT)$].

inset of Fig. 3. However, by inspecting the plot of $d\rho/dT$ versus $\log_{10}T$ in Fig. 9(a), one sees that passing from B_c-type crystal 1, through A_a-type No. 5, to A_b-type one No. 9, the temperature ranges of the "impurity" sections 1 and 2 gradually expand until they completely occupy the intrinsic regions: i.e., the activation section 3 for A_b-type crystals. Furthermore, the data series of $[\rho_0;+T_{d1}]$, $[\rho(T_{d1});+T_{d1}]$, and $[\rho(T_{d2});+T_{d2}]$ each follow an Arrhenius equation, while the T_{d3} characteristic temperature vanishes for crystals 4–9. The inset to Fig. 9(a) shows $\log_{10}\rho_0$ versus $1/T_{d1}$. The straight line in the inset represents $\Delta_0/k_B \approx 100$ K. For the subsequent series, the value of Δ_0/k_B decreases. The data are plotted in Fig. 10 (large crosses) and are approximated by the corresponding Arrhenius equations (lines).

The data presented in Fig. 9 and the above description can be summarized as follows. All of the $CeFe_4As_{12}$ crystals examined belong to the same semiconducting state but contain different densities of stoichiometric defects. However, the concentration of defects is low enough to allow the lattice parameters and intrinsic electronic structure to remain roughly constant. The stoichiometric defects, which vary the carrier concentration in A_b-type crystals, are sufficiently high to provide semimetallic conductivity. With reduction of the defects and, hence, impurity carrier conductivity in A_a- and B_c-type crystals, the intrinsic activation behavior is increasingly revealed.

However, we also point out that the trends presented in Fig. 3 resemble the effect of La substitution in the series $(Ce_{1-x}La_x)_3Bi_4Pt_3$ on the electrical resistivity and thermoelectric power[41] or the calculated resistivity for different concentrations of non-*f* impurity atoms replacing *f*-electron atoms.[42] Although we do not have clear evidence for replacing *f*-electron atoms with non-*f*-electron atoms in the case of $CeFe_4As_{12}$, we do have evidence for sample-dependent Hall carrier concentrations, which presumably are due to some different sort of undefined stoichiometric defects. The above analyses of the electrical resistivity for $CeFe_4As_{12}$ are based on textbook formulas appropriate for semiconductors obeying Boltzmann statistics [Eqs. (3) and (3a)]. However, better quantitative analysis at higher temperatures should employ degenerate semiconductor electron statistics,[41,43,44] because $CeFe_4As_{12}$ is in the degenerate ($E_g \approx k_BT$) limit. As for the previous analyses, the electronic structure is modeled as two sides of parabolic bands of equal mass separated by $E_g(T)$ (with E_g an indirect gap). For these assumptions, the expression for the resistivity is given by:[41,43,44]

$$\rho(T) = \rho_0/\ln[1 + \exp(-E_g/k_BT)], \tag{4}$$

where ρ_0 is a constant, k_B is the Boltzmann constant ("lnX" means "$\log_e$X"). This approach yields values for E_g that can be approximated in units of K as $E_g = 403-2.12 \times T$ for temperatures 130 K $\leqslant T \leqslant$ 155 K. This slope is over twice as large as the highest value observed for hybridization gap semiconductor $Ce_3Bi_4Pt_3$.[43] The latter dependence determined in the wider temperature range was found to be consistent with a mean-field prediction[45] based on the Anderson lattice Hamiltonian. The predicted $E_g(T)$ saturates at 148 K for $T \to 0$ K. Comparing $E_g(T)$ for $CeFe_4As_{12}$ to $E_g(T)$'s determined[43] and predicted[45] for $Ce_3Bi_4Pt_3$, we might speculate that the saturated value of $E_g(0)$ for $CeFe_4As_{12}$ is rather closer to the value $E_g(0) = 330$ K determined with Eq. (3a) than to $E_g(0) = 403$ K determined by the linear extrapolation of $E_g(T)$ from the 130 K $\leqslant T \leqslant$ 155 K range to $T \to 0$ K.

The Hall carrier mobility μ_H is presented in Fig. 9(b). The lowest curve in this figure presents $\mu_H(T)$ for crystal 8. The saturated value of $\mu_H(0) = 115$ cm^2/Vs remains temperature independent up to 20 K, as seen for the residual resistivity in metals. Then the mobility starts to decrease with an increasing rate that is stronger than predicted ($\mu \sim T^{-1}$) for simple metals above $\Theta_D/2$[46] due to phonon scattering. The saturated mobility of semiconducting crystals increases to about 149 cm^2/Vs due to increasing purity and then increases by about 15% with increasing temperature, passes through a maximum at about 100 K, and decreases again by about 15% at 155 K. This weak temperature dependence supports the credibility of our low-temperature resistivity analysis. The maximum of $\mu(T)$ is a characteristic feature of a semiconductor if it simultaneously has both charged impurity scattering $\mu_I(\sim T^{3/2})$ and acoustic lattice scattering $\mu_L(\sim T^{-3/2})$ (Ref. 47) controlling the carrier scattering on the low- and high-temperature sides of the maximum, respectively. The 3/2 exponent is reduced, presumably due to the large contribution of the temperature independent scattering on the low-temperature side. On the other hand, the $-3/2$ exponent is exceeded when room temperature is

approached. The stronger increase of μ_H compared to the decrease of charge carrier density with decreasing temperature, shifts the temperature of the resistivity minimum down to 165 K. This description explains the inconsistency between the resistivity and susceptibility points separating the low- and high-temperature regions.

The thermopower, if it is interpreted in terms of an expression for a simple one-band model of carriers of charge e and Fermi energy E_F, is given by

$$S = \pi^2 k_B^2 T/2eE_F. \quad (5)$$

We expect from Eq. (5) a peak of $S(T)$ as a result of the increase of $S(T)$ with increasng temperature which, in turn, causes an increase of the carrier concentration; i.e., a decrease of R_H, and hence $1/E_F$. Thus the decrease of $S(T)$ with increasing temperature reflects the dominant effect of the decrease of R_H on $S(T)$ between $T_{\max}$ and $T_{\min}$. This is the range in which the dominant effect is the electron activation through the energy gap. The increasing value and slope of $S(T)$ between $T_{\max}$ and $T_{\min}$ for decreasing sample number is roughly consistent with what we might expect from examination of the Hall effect data on the basis of Eq. (5). However, $S(T) < 0$ below about 4 K is unexpected on the basis of Eq. (5), and the behavior of R_H is presumably due to a more complex electronic structure due to stoichiometry defect levels (or impurity bands) inside the energy gap of the crystal. However, Behnia *et al.*[48] argue that, independent of complex structure and contributions from different carriers, in the zero-temperature limit the thermoelectric power should obey the universal relation:

$$q = (S/T)(N_A e/\gamma), \quad (6)$$

where N_A is Avogadro's number and the product $N_A e = 9.65 \times 10^4$ C/mole is the Faraday number.[48] The dimensionless quantity q corresponds to the density of carriers per formula unit for the case of a free electron gas with an energy independent relaxation time. (Zlatić *et al.*[49] derived Eq. (6) more rigorously.) In a wide range of different metals, Behnia *et al.*[48] found $0.5 < |q| < 2$, and, in other cases, the number of carriers per formula unit gives a satisfactory explanation for the magnitude of q. For instance, $q \sim 107$ for the Kondo insulator CeNiSn, for which the carrier density <0.01 e^-/f.u. below 5 K.[48] Shown in left inset of Fig. 5 are $S(T)$ data for crystals B_c; No. 1 (circles), A_a; No. 5 (diamonds), and A_b; No. 8 (dotted circles) with solid lines showing the slopes at the lowest temperatures. Here, S/T equals 1.22, 0.45, and -0.29 μV/K^2, respectively. Using these values, as well as γ (3.3 mJ/mole K^2 determined for A_a or B_c crystals and 3.1 mJ/mole·K^2 determined for A_b crystals), the dimensionless quantity q is calculated to be 36, 13, and -9.0 for B_c, A_a, and A_b crystals, respectively, consistent with increasing carrier density of the crystals examined. These values can be compared with $q = 89$ determined for a hybridization gap semiconductor, the filled skutterudite $CeOs_4As_{12}$, for which the electrical resistivity increases by over two orders of magnitude[8] and the carrier density decreases by over three orders[9] of magnitude with decreasing temperature from 100 K to 1 K. Lower values of q were found for other filled skutterudite arsenides: (i) $CeRu_4As_{12}$ where $q \approx -2.2$ in the non-Fermi liquid state,[11] (ii) $PrFe_4As_{12}$ (ferromagnetic metal) where the zero-field value of $q \approx -0.3$,[50] and (iii) $PrRu_4As_{12}$ (superconductor below about 2.5 K) where $q \approx -0.3$ to -0.5.[29] All of these arsenide skutterudites have positive thermoelectric power values at room temperature.

It is interesting to note that despite the fact that representative examples (e.g., crystal No. 8) of the A_b-type crystals, which show carrier densities that are larger by a factor of over 3 over those B_c-type crystals (e.g., crystal No. 2), they have the same values of $\gamma = 3.3$ mJ/mole K^2. Such values for γ are quite high in comparison to conventional semiconductors and low in comparison to typical correlated electron systems. Therefore, we presume that they do not represent the Hall carrier concentration. On the other hand, the values of Θ_D, equal to 580 K for these two type crystals, are large in comparison to other filled skutterudites, although a theoretical Ref. 14 gives an even higher $\Theta_D = 635$ K calculated for $CeFe_4As_{12}$. It might be useful to compare our data to a few other La and Ce based filled skutterudites. Values of Θ_D determined for $LaFe_4As_{12}$ by heat capacity or thermal expansion measurements equal 322 (Ref. 51) or 470 K.[48,52] Heat capacity measurements of $CeRu_4As_{12}$ and CeO_4As_{12} yielded values of Θ_D of 156 (Ref. 11) and 264 K,[8] respectively. Based on powder diffraction and transport properties studies, we conclude that the peak is probably due to small amounts of crystalline clusters of magnetic impurity phase that contribute their heat capacity to C_p of crystals of A_a-type examined.

Many authors employ the Anderson lattice model for a basic description of the electronic properties of heavy-fermion materials and Kondo semiconductors.[53] This theory predicts an indirect gap in the density of states, where the chemical potential lies directly in the gap. The bottom of the conduction band and the top of the valence band have high density of states, which is mostly of *f* character. The gaps in the Kondo semiconductors are extremely sensitive to doping, in which the *f* ions are substituted by non-*f* ions.[42] Our results for band structure calculations are consistent with results of Nordström and Singh[54] for $CeFe_4P_{12}$ and $CeFe_4Sb_{12}$. They predict, as expected for Kondo semiconductors, a high density of states that is mostly *f*-like at the bottom of the conduction band. However, the top of the valence band is formed by a low density of states parabolic band that, for $CeFe_4As_{12}$, is situated roughly $E_g \sim 0.20$ eV below the conduction band. This value is between $E_g = 0.34$ and 0.10 eV, as found for $CeFe_4P_{12}$ and $CeFe_4Sb_{12}$, respectively.[54] It is, however, interesting that for all three compounds at the same energy distance, 0.4 eV below the conduction band, there is another parabolic band with hybridized states with 4*f* character. We may speculate that the weak effect of the low-temperature charge carrier density on E_g is due to non-4*f* character of the defect acceptor state located over non-4*f* character states at the top of the valence band. On the other hand, deeper in the valence band, the 4*f* hybridized states may be responsible for the strong temperature dependence of E_g. Our band structure calculations for $CeFe_4As_{12}$ are roughly consistent with those of Ref. 14, which do not reveal details related to electron transport and hybridization properties. We can compare our experimentaly determined lattice parameter $a = 8.302$ Å and calculated $E_g = 0.20$ eV to those of Ref. 14 calculated for $CeFe_4As_{12}$,

$a = 8.146$ Å and $E_g \approx 0.24$ eV, while from our $E_g(a)$ (see Fig. 8) one finds $E_g \approx 0.26$ eV for $a = 8.146$ Å. These are negligible differences as compared to the values (determined here) $E_g(0) \approx 330$ K (0.028 eV) and overestimate the band gaps calculated using the LDA method.

It is also worthwhile to draw comparisons to other Ce-filled skutterudite arsenides. $CeRu_4As_{12}$, when obtained by a high-temperature, high-pressure technique, was reported to be semiconducting with an activation energy of 50 K as determined from electrical resistivity data, which increase by about 25% for $90\ K > T > 55$ K.[10] The magnetic susceptibility of this sample showed a broad maximum around 270 K. The activation energy of 15 meV (174 K) has also been reported for a cold-pressed pellet of $CeRu_4As_{12}$ by a two-probe technique.[13] On the other hand, electrical resistivity, thermoelectric power, specific heat, and magnetic measurements made on single crystals of $CeRu_4As_{12}$, grown by flux method, revealed a semi-metallic non-Fermi liquid state.[11] It is also worth mentioning that the skutterudite $La_{0.48}Rh_4As_{12}$, in which the rare-earth sites are nearly half filled with a non-*f* electron rare-earth element La, is a semiconductor with an energy gap of 0.03 eV,[55] while the compound $LaRu_4As_{12}$ in which the rare-earth sites are completely filled with La atoms, is superconducting below 10.3 K.[56] This result seems to show that the semiconducting properties of the skutterudite arsenides are not necessarily due to the hybridization of filling atom *f*-electron and band electron states.

The most explicit case among the Ce-filled skutterudite arsenides was found for $CeOs_4As_{12}$, where an increase of the electrical resistivity over two orders[8] of magnitude and a decrease of Hall carrier concentration from 7×10^{20} to $1.5 \times 10^{17} e^+/cm^3$ were observed with decreasing temperature from RT down to 0.3 K (resistivity saturation).[9] An examination revealed that these phenomena are associated with *f*-electron-conduction electron hybridization. Valence fluctuations or Kondo behavior dominates the physics down to $T \sim 135$ K. The correlated electron behavior is manifested at low temperatures as a hybridization-gap insulating state. The small energy gap $\Delta/k_B \sim 73$ K, taken from fits to electrical resistivity data, correlates with the evolution of a weakly magnetic or nonmagnetic ground state, which is evident in the magnetization data below a coherence temperature $T_{coh} \sim 45$ K. The nonmagnetic analogue compound $LaOs_4As_{12}$ shows decreasing magnetic susceptibility with increasing temperature, which is smaller than that of $CeOs_4As_{12}$ over the entire temperature range. We find the opposite case when Os is replaced by Fe. The $\chi(T)$ of $CeFe_4As_{12}$ is lower than that for $CeOs_4As_{12}$ and still decreases for temperature decreasing below ~280 K. It is also lower than the susceptibility of $LaFe_4As_{12}$, which even becomes ferromagnetic below 3.8 K. This raises the first question of how the magnetism of the Fe ions affects the magnetic behavior of $CeFe_4As_{12}$. On the other hand, the electronic specific heat of $CeFe_4As_{12}$ [$\gamma \sim 3.3$ mJ/K^2 mole] is higher than that of conventional semiconductors, but is about 6 times lower from that in $CeOs_4As_{12}$ and the γ-related paramagnetic contribution may not so greatly dominate the possible diamagnetic contribution to the magnetic susceptibility for $T < 300$ K in $CeFe_4As_{12}$. Therefore we suggest that either magnetism of the Fe ions or the possible diamagnetic contribution may be responsible for the weak decrease of $\chi(T)$ of $CeFe_4As_{12}$ below ~280 K. This may also cause the weakness of some features that may be related to those clearly visible in $\chi(T)$ for $CeOs_4As_{12}$ that originate in the propensity of the Ce ion to exhibit intermediate valence or Kondo behavior that results in a hybridization-gap insulating state.

Finally, we point out that the temperatures containing the flat peak of $\chi\ (T)$ and below obviously correspond to the extrinsic regimes (1) and (2) where the conductivity is dominated by impurity states in the gap. The monotonically decreasing value or slope of R_H up to RT shows no sign of an anomaly at $T_M \approx 165$ K, assumed to be due to a metal-hybridization-gap semiconductor transition because of the resistivity minimum. However, we should mention the increase of the slope of $\chi(T)$ for $T > 300$ K as a possible transition to regime (1) where intermediate valence effects are dominant. Simply speaking, the c-*f* hybridization increasing the density of states of the conduction band with 4*f* electron states, releases electrons that fill up the valence band, thus disclosing the hybridization-dependent energy gap. Then it is possible to observe the activation processes in regime (3), dependent on the density of stoichiometric defects, the origin of acceptor states is mainly responsible for the *p*-type conductivity.

We conclude that the filled skutterudite compound $CeFe_4As_{12}$ is a hybridization-gap semiconductor ($E_g \approx$ 28 meV) below a continuous transition from a metallic to a semiconducting state, which is not associated with a structure change. Presumably, the transition starts at ~280−300 K, but the expected minimum of the resistivity caused by this transition is shifted to $T_M = 165$ K due to a rapid increase of carrier mobility in this range. The decrease of impurity states in the gap reveals the semiconducting state of $CeFe_4As_{12}$ below T_M. However, a minority of crystals is found to exhibit semimetallic behavior, but they form only under specific conditions. From the point of view of electrical transport in $CeFe_4As_{12}$, the temperature range can be divided into several regimes that are dominated by various mechanisms: for $T > T_{d3}$ the electron-phonon scattering dominates, the third regime for $T_{d2} < T < T_{d3}$ where the main contribution is the activation process, and the second and first ones for $T_{d1} < T < T_{d2}$ and $T < T_{d1}$, respectively, the so-called extrinsic regime where impurity states are dominant (conductivity saturates). The compound $CeFe_4As_{12}$ is weakly magnetic and an increase of the magnetic susceptibility with temperature suggests an intermediate valence state for the Ce ions. The Kondo picture with a high Kondo temperature (1000−1260 K) is also considered. In particular, our band structure calculation confirmed the value of the gap estimated by using the above mentioned model. Examination of the Hall effect and thermoelectric power reveals, with one exception, a positive sign of the majority of charge carriers. The maximum of the Hall mobility at low temperatures also confirms the semiconducting character of $CeFe_4As_{12}$.

ACKNOWLEDGMENTS

Research at ILTSR, R. W. was supported by the Polish Ministry of Science and Higher Education (Grant No. N N202 4129 33). Research at UCSD was supported by the US Department of Energy (Grant No. DE-FG02-04ER46105).

[1]M. B. Maple, E. D. Bauer, N. A. Frederick, P.-C. Ho, W. M. Yuhasz, and V. S. Zapf, Physica B **328**, 29 (2003).
[2]Y. Aoki, H. Sugawara, H. Harima, and H. Sato, J. Phys. Soc. Jpn. **74**, 209 (2005).
[3]M. B. Maple, Z. Henkie, R. E. Baumbach, T. A. Sayles, N. P. Butch, P.-C. Ho, T. Yanagisawa, W. M. Yuhasz, R. Wawryk, T. Cichorek, and A. Pietraszko, J. Phys. Soc. Jpn. **77** Suppl. A, 7 (2008).
[4]H. Sato, D. Kikuchi, K. Tanaka, M. Ueda, H. Aoki, T. Ikeno, S. Tatsuoka, K. Kuwahara, Y. Aoki, M. Kohgi, H. Sugawara, K. Iwasa, and H. Harima, J. Phys. Soc. Jpn. **77** Suppl. A, 1 (2008).
[5]H. Sugawara, S. Osaki, M. Kobayashi, T. Namiki, S. R. Saha, Y. Aoki, and H. Sato, Phys. Rev. B **71**, 125127 (2005).
[6]D. J. Braun and W. Jeitschko, J. Solid State Chem. **32**, 357 (1980).
[7]D. J. Braun and W. Jeitschko, J. Less-Common Metals **72**, 147 (1980).
[8]R. E. Baumbach, P.-C. Ho, T. A. Sayles, M. B. Maple, R. Wawryk, T. Cichorek, A. Pietraszko, and Z. Henkie, PNAS **105**, 17307 (2008).
[9]R. Wawryk (private communication).
[10]C. Sekine, N. Hoshi, K. Takeda, T. Yoshida, I. Shirotani, K. Matsuhira, M. Wakeshima, and Y. Hinatsu, J. Magn. Magn. Mater. **310**, 260 (2007).
[11]R. E. Baumbach, P.-C. Ho, T. A. Sales, M. B. Maple, R. Wawryk, T. Cichorek, A. Pietraszko, and Z. Henkie, J. Phys. Condens. Matter **20**, 075110 (2008).
[12]A. Watcharapasorn, R. S. Feigelson, T. Ceillat, A. Borshchevsky, G. J. Snyder, and J.-P. Fleurial, J. Appl. Phys. **91**, 1344 (2002).
[13]F. Grandjean, A. Gérard, D. J. Braun, and W. Jeitschko, J. Phys. Chem. Solids **45**, 877 (1984).
[14]M. Hachemaoui, R. Khenata, A. Bouhemadou, Ali H. Reshak, D. Rached, and F. Semari, Curr. Opin. Solid State Mater. Sci. **13**, 105 (2009).
[15]R. Wawryk, Z. Henkie, A. Pietraszko, T. Cichorek, A. Jezierski, R. E. Baumbach, and M. B. Maple, J. Phys.: Conf. Ser. **200**, 12223 (2010).
[16]Z. Henkie, M. B. Maple, A. Pietraszko, R. Wawryk, T. Cichorek, R. E. Baumbach, W. M. Yuhasz, and P.-C. Ho, J. Phys. Soc. Jpn. **77**, Suppl. A, 128 (2008).
[17]G. M. Sheldrick, *Program for the Solution of Crystal Structures* (University of Göttingen, Germany, 1985).
[18]G. M. Sheldrick, *Program for Crystal Structure Refinement* (University of Göttingen, Germany, 1987).
[19]R. Wawryk and Z. Henkie, Phil. Mag. B **81**, 223 (2001).
[20]B. Nowak, O. Żogał, A. Pietraszko, R. E. Baumbach, M. B. Maple, and Z. Henkie, Phys. Rev. B **79**, 214411 (2009).
[21]K. Koepernik and H. Eschrig, Phys. Rev. B **59**, 1743 (1999).
[22]I. Opahle, K. Koepernik, and H. Eschrig, Phys. Rev. B **60**, 14035 (1999).
[23]J. P. Perdew and Y. Wang, Phys. Rev. B **45**, 13244 (1992).
[24]N. Kurita, M. Hedo, M. Koeda, M. Kobayashi, H. Sato, H. Sugawara, and Y. Uwatoko, Phys. Rev. B **79**, 014441 (2009).
[25]M. B. Maple and D. Wohlleben, Phys. Rev. Lett. **27**, 511 (1971).
[26]M. B. Maple and D. Wohlleben, *Magnetism and Magnetic Materials*, AIP Conf. Proc. 1073, No. 18, edited by C. D. Graham Jr. and J. J. Rhyne (New York, AIP, 1974), p. 447.
[27]A. C. Hewson, *The Kondo Problem to Heavy Fermions* (Cambridge University Press, Cambridge, UK, 1993).
[28]D. A. Gajewski, N. Dilley, E. D. Bauer, E. J. Freeman, R. Chau, M. B. Maple, D. Mandrus, B. C. Sales, and A. H. Lacerda, J. Phys. Condens. Matter **10**, 6973 (1998).
[29]P. A. Rayjada, A. Chainani, M. Matsunami, M. Taguchi, S. Tsuda, T. Yokoya, S. Shin, H. Sugawara, and H. Sato, J. Phys. Condens. Matter **22**, 095502 (2010).
[30]N. F. Mott and W. D. Twose, Adv. Phys. **10**, 107 (1961).
[31]P. J. Markowski, Z. Henkie, and A. Wojakowski, Solid State Commun. **32**, 1119 (1979).
[32]T. A. Sayles, R. E. Baumbach, W. M. Yuhasz, M. B. Maple, Ł. Bochenek, R. Wawryk, T. Cichorek, A. Pietraszko, Z. Henkie, and P.-C. Ho, Phys. Rev. B **82**, 104513 (2010).
[33]M. Očko, C. Gaibel, and F. Steglich, Phys. Rev. B **64,** 195107 (2001).
[34]N. F. Mott, *Metal-Insulator Transitions* (Taylor and Francis, London, 1990).
[35]B. I. Shklovskii and A. L. Efros, *Electronic Properties of Doped Semiconductors*, edited by M. Cardona (Springer, Berlin, 1984).
[36]Z. Henkie and P. Markowski, J. Phys. Chem. Solids **39**, 39 (1978).
[37]I. Mörke, J. Schoenes, M. Küng, Z. Henkie, and P. Wachter, Helv. Phys. Acta **56**, 915 (1983).
[38]J. Schoenes, M. Küng, R. Hauert, and Z. Henkie, Solid State Commun. **47**, 23 (1983).
[39]D. T. Morelli and G. P. Meisner, J. Appl. Phys. **77**, 3777 (1995).
[40]I. Mori, H. Sugawara, K. Magishi, T. Saito, K. Koyama, D. Kikuchi, K. Tanaka, and H. Sato, J. Magn. Magn. Mat. **310**, 277 (2007).
[41]M. F. Hundley, P. C. Canfield, J. D. Thompson, and Z. Fisk, Phys. Rev. B **50**, 18142 (1994).
[42]P. S. Riseborough, Phys. Rev. B **68**, 235213 (2003).
[43]M. F. Hundley, P. C. Canfield, J. D. Thompson, and Z. Fisk, Physica B **199 & 200**, 443 (1994).
[44]D. R. Lovet, *Semimetals and Narrow-Band Gap Semiconductors* (Pion, London, 1977), p. 72.
[45]C. Sanchez-Castro, K. S. Bedell, and B. R. Cooper, Phys. Rev. B **47**, 6879 (1993).
[46]G. W. Webb, Phys. Rev. **181**, 1127 (1969).
[47]R. H. Bube, *Electrons in Solids* (Academic Press, Boston, 1988), p. 172.
[48]K. Behnia, D. Jaccard, and J. Flouquet, J. Phys. Condens. Matter **16**, 5187 (2004).
[49]V. Zlatić, R. Monnier, J. K. Freericks, and K. W. Becker, Phys. Rev. B **76**, 085122 (2007).
[50]T. A. Sayles, W. M. Yuhasz, J. Paglione, T. Yanagisawa, J. R. Jeffries, M. B. Maple, Z. Henkie, A. Pietraszko, T. Cichorek, R. Wawryk, Y. Nemoto, and T. Goto, Phys. Rev. B **77**, 144432 (2008).
[51]S. Tatsuoka, H. Sato, K. Tanaka, M. Ueda, D. Kikuchi, H. Aoki, T. Ikeno, K. Kuwahara, Y. Aoki, H. Sugawara, and H. Harima, J. Phys. Soc. Jpn. **77**, No. 3, 033701 (2008).
[52]G. Rogl, L. Zhang, P. Rogl, A. Grytsiv, M. Falmbigl, D. Rajs, M. Kriegisch, H. Müller, E. Bauer, J. Koppensteiner, W. Schranz, M. Zehetbauer, Z. Henkie, and M. B. Maple, J. Appl. Phys. **107**, 043507 (2010).
[53]P. S. Riseborough, Adv. Phys. **49**, 257 (2000).
[54]L. Nordström and D. J. Singh, Phys. Rev. B **53**, 1103 (1996).
[55]K. Arii, H. Takahashi, H. Okada, H. Takahashi, M. Imai, T. Aoyagi, T. Kimura, C. Sekine, J. Hayashi, and I. Shirotani, J. Phys. Conf. Ser. **215**, 012032 (2010).
[56]I. Shirotani, T. Uchiumi, K. Ohno, C. Sekine, Y. Nakazawa, K. Kanoda, S. Todo, and T. Yagi, Phys. Rev. B **56**, 7866 (1997).